Mat. Res. Soc. Symp. Proc. Vol. 621 © 2000 Materials Research Society

Nd:YVO_4 Laser Crystallization for Thin Film Transistors with a High Mobility

Ralf Dassow[1], Jürgen R. Köhler[1], Melanie Nerding[2], Horst P. Strunk[2], Youri Helen[3], Karine Mourgues[3], Olivier Bonnaud[3], Tayeb Mohammed-Brahim[3], and Jürgen H. Werner[1]
[1]Universität Stuttgart, Institut für Physikalische Elektronik, Pfaffenwaldring 47, D-70569 Stuttgart, Germany, r.dassow@ipe.uni-stuttgart.de
[2]Universität Erlangen-Nürnberg, Institut für Werkstoffwissenschaften, Lehrstuhl für Mikrocharakterisierung, Cauerstr. 6, D-91058 Erlangen, Germany
[3]Groupe de Microélectronique et Visualisation, Université de Rennes 1, Campus de Beaulieu, F-35042 Rennes Cedex, France

ABSTRACT

We crystallize amorphous silicon films with a frequency doubled Nd:YVO_4 laser operating at a repetition frequency of up to 50 kHz. A sequential lateral solidification process yields polycrystalline silicon with grains longer than 100 µm and a width between 0.27 and 1.7 µm depending on film thickness and laser repetition frequency. The average grain size is constant over the whole crystallized area of 25 cm^2. Thin film transistors with n- type and p-type channels fabricated from the polycrystalline films have average field effect mobilities of μ_n = 467 cm^2/Vs and μ_p = 217 cm^2/Vs respectively. As a result of the homogeneous grain size distribution, the standard deviation of the mobility is only 5 %.

INTRODUCTION

Polycrystalline silicon fabricated at low temperatures is of great interest for future electrical devices on cheap and /or transparent substrates (e. g. glass). Laser crystallization of amorphous silicon deposited at low temperatures is the most promising technique to produce the desired material with excellent electrical properties. The established process is based on the irradiation of each part of the silicon film with a number of n = 10 ... 50 pulses of an excimer laser [1]. To improve the electrical properties of the devices, crystallization of the active layer is often performed in vacuum [2]. Thin film transistors (TFTs) with the highest reported electron mobility μ = 640 cm^2/Vs were deposited and crystallized completely in ultra high vacuum [3]. Unfortunately, with the established processes the grain sizes and therefore also (due to grain boundaries [4]) the electrical properties of the TFTs depend strongly on the laser's local energy density D. For example, an increase of D from D = 406 mJ/cm^2 to D = 420 mJ/cm^2 results in a decrease of the grain size d from d = 500 nm to d = 30 nm [5]. Due to this sensitivity of d on D, temporal and spatial fluctuations of the laser energy lead to considerable scatter in TFT properties. Sequential lateral solidification (SLS) increases the grain size [6] and hence reduces the number of grain boundaries within the devices. This reduction should significantly improve the electrical properties. Simultaneously the SLS process reduces the sensitivity of the grain size on the energy density D. Unfortunately, up to now only excimer lasers were used in combination with an SLS process. The repetition rate of this type of laser has an upper limit of f ≈ 300 Hz. As a consequence the crystallization process is slow.

This work presents the results of non-vacuum laser crystallization utilizing an SLS process in

combination with a Nd:YVO_4 laser operating at a repetition rate of up to 50 kHz. We produce n- and p-channel thin film transistors with average field effect mobilities of $\mu_n = 467$ cm^2/Vs and $\mu_p = 217$ cm^2/Vs, for electrons and holes respectively. The structural homogeneity of our film results in a standard deviation for the field effect mobility of only 5%.

EXPERIMENTAL DETAILS

Silicon Deposition

We use two different types of samples for our crystallization experiments. Sputtering deposits silicon films with different film thicknesses d = 50 ... 300 µm on 5 x 5 cm^2 Corning 1737F glass. With these films, we investigate the influence of d and of the crystallization parameters on the crystalline structure. Further, we deposit an a-Si layer with a thickness of d = 150 nm by low pressure chemical vapor deposition (LPCVD) on a SiO_2 buffer layer. The SiO_2 serves as a diffusion barrier and is deposited on a 5 x 5 cm^2 HOYA NA 40 glass substrate by atmospheric pressure chemical vapor deposition (APCVD). Further details of the deposition technique were given in Ref. [7].

Laser Crystallization

Figure 1 shows the experimental setup for the crystallization of the amorphous silicon film with a pulsed Nd:YVO_4 laser. The laser emits light with a wavelength $\lambda = 532$ nm at a tunable repetition frequency f < 100 kHz. Beam shaping of the TEM_{00} beam with one cylindrical and one spherical lens forms an elliptical beam cross section at the surface of the substrate. The energy density has a Gaussian height h = 12 µm in x-direction and a width w = 460 µm in the perpendicular y-direction. A translation stage moves the sample with a scanning speed v in x-direction. The stage limits v to the maximum speed $v_{max} = 25$ cm/s. Between each pulse of the laser the sample is translated by a distance $\Delta x = v / f$. We tune the repetition frequency f to the scanning speed v to obtain a translation $\Delta x = 0.5$ µm. In our experiments we use the scanning velocities v = 10 mm/s and v = 25 mm/s with the corresponding repetition frequencies f = 20 kHz and f = 50 kHz respectively.

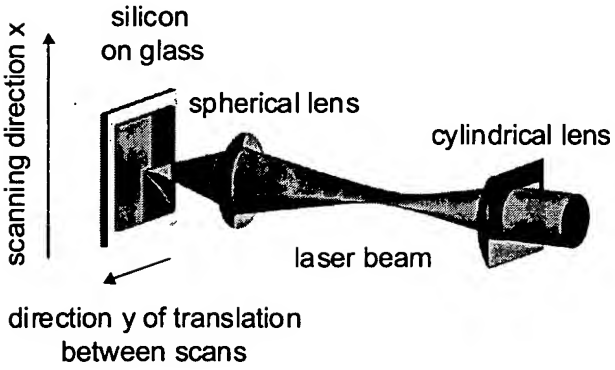

Figure 1. Experimental setup. A cylindrical and a spherical lens shape the TEM_{00} laser beam to form an elliptical beam cross section at the surface of the substrate.

The laser pulse energy E is adjusted to completely melt an elliptical area with a width $w_m = 200$ µm and a height $h_m = 5$ µm. Table I shows the required energy E for films with a different thickness d. The maximum pulse energy of our Nd:YVO_4 laser decreases from $E_{max} \approx 100$ µJ to at $E_{max} \approx 10$ µJ as the frequency f increases from f = 10 kHz to f = 100 kHz. Therefore, we reduced the film thickness to crystallize samples at high repetition frequencies. With the maximum scanning speed $v_{max} = 25$ cm/s and the corresponding f = 50 kHz the pulse

Table I. Pulse energy E required to completely melt an elliptical area with the width w_m = 200 μm and the height h_m = 5 μm for silicon films on glass with a different thickness d.

Film Thickness d (nm)	50	75	150	300
Pulse Energy E (μJ)	12.4	14.6	20.4	27.9

energy is sufficient to crystallize a silicon film with a maximum thickness d = 50 nm.

As the film cools after the laser pulse, lateral growth proceeds from the edges of the completely molten area [6]. The next laser pulse again melts an elliptical area, which is translated by the distance Δx = 0.5 μm with respect to the previous one. Now the edge of the completely molten area is located within the laterally grown grains produced by the previous step. Hence these grains act as seed and are elongated as the film cools. Repeating the pulsed laser irradiation during the translation of the sample results in long elongated grains with a length l exceeding by far the single pulse lateral growth length $\Delta l \approx 1$ μm [8].

After a completed scan in x-direction, we translate the sample by a distance Δy = 130 μm in y-direction. The distance y is smaller than the width w_m of the complete molten area to have an overlap between to subsequent scans.

RESULTS

Transmission Electron Microscopy

We investigate the influence of the film thickness d and the laser repetition frequency f on the crystalline structure of the films with transmission electron microscopy (TEM). Figures 2a to 2d show grains which are elongated in the scanning direction of the SLS process. The grain width increases with increasing d (see Figs. 2a to 2c) and also with a increasing f (see Figs 2a, 2d). We calculate the average grain width w_G of the different samples by evaluating a large number of TEM pictures. Figure 2e shows an increase from w_G = 0.27 μm to w_G = 1.7 μm as the film thickness d increases from d = 50 nm to d = 300 nm.

The almost linear increase of the grain width w_G correlates with the influence of the film thickness d on the melt duration t_m. Our numerical analysis using a two-dimensional thermodynamic computer simulation [9] shows that an increase from d = 50 nm to d = 300 nm results in an almost linear increase of the melt duration from t_m = 43 ns to t_m = 208 ns. Therefore, we attribute the increase in the grain width w_G to the increase of t_m, which means that the grains have more time to grow and therefore w_G increases. The grain width parameter

$$w_t = \frac{dw_G}{dt_m} \tag{1}$$

represents the increase of w_G per increase of t_m. Using our experimental and simulation results we calculate $w_t \approx \Delta w_G / \Delta t_m$ = (300 – 50) nm / (208 – 43) nm = 8.7 nm/ns.

Figure 2e shows an increase from w_G = 0.27 μm to w_G = 0.45 μm as the laser frequency increases from f = 20 kHz to f = 50 kHz using 50 nm thick films. At the same time the pulse energy density D_m required for completely melting the silicon decreases by about 12 %. Again an increase of the melt duration t_m, now caused by an increasing temperature of the silicon film, explains the raising of w_G as well as the decrease of D_m: i) Our numerical simulations indicate that a reduction of D_m by 12 % is a result of an increase of the silicon film temperature T prior to

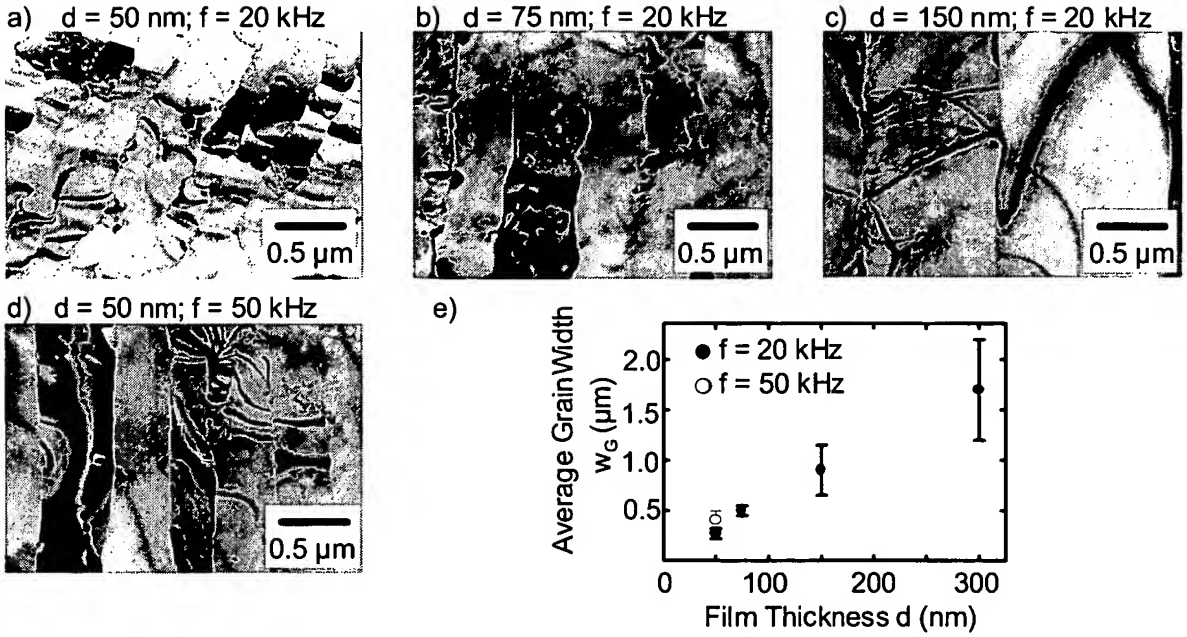

Figure 2: a) - c) TEM pictures of samples with a film thickness d = 50 ... 150 crystallized with a repetition frequency f = 20 kHz. d) TEM picture of a sample with d = 50 nm crystallized at f = 50 kHz. e) The average grain width w_G increases with increasing film thickness d and increasing repetition frequency f.

the onset of the laser pulse from T = 300 K to T = 660 K. ii) By inserting the enhanced silicon temperature T = 660 K into our simulation, we obtain an increase of this melt duration from t_m = 43 ns to t_m = 65 ns. The increasing temperature t_m of the silicon film can be explained by a rise of the average laser beam power as the frequency f increases at a constant pulse energy E. Now we calculate the grain width parameter $w_t \approx (0.45 - 0.27)$ nm / (65 - 43) ns = 8.2 nm/ns.

The grain width parameters w_t are approximately the same in the two considered cases of film thickness variation and temperature variation due to different repetition frequencies f.

Homogeneity

We investigate the homogeneity and the crystalline structure of the laser crystallized samples with optical and scanning electron microscopy (SEM). The bottom part of Fig. 3a shows a sample after Secco etching. A single laser scan with an energy density distribution shown in the upper part of Fig. 3a crystallized the silicon. Secco etching not only removes the silicon at the defects of the crystalline structure, but also affects the glass due to the HF content of the solution. The latter effect results in a lift-off of small grained silicon. Only large grains produced by the SLS process remain on the glass and appear as bright areas in the optical microscope. In the center of the laser beam, where the energy density D is higher than the energy density D_m, which is required for complete melting, the SLS process results in long elongated grains. D_m is the energy density required to completely melt crystalline silicon. The region of the large grained silicon has a width $w_{LG} \approx 200$ µm. In the outer part of the laser beam with an energy density $D < D_m$ the silicon film is not melted completely. The resulting grain size depends on the local energy density, but is smaller than the film thickness d [10]. These regions appear as dark areas in Fig.

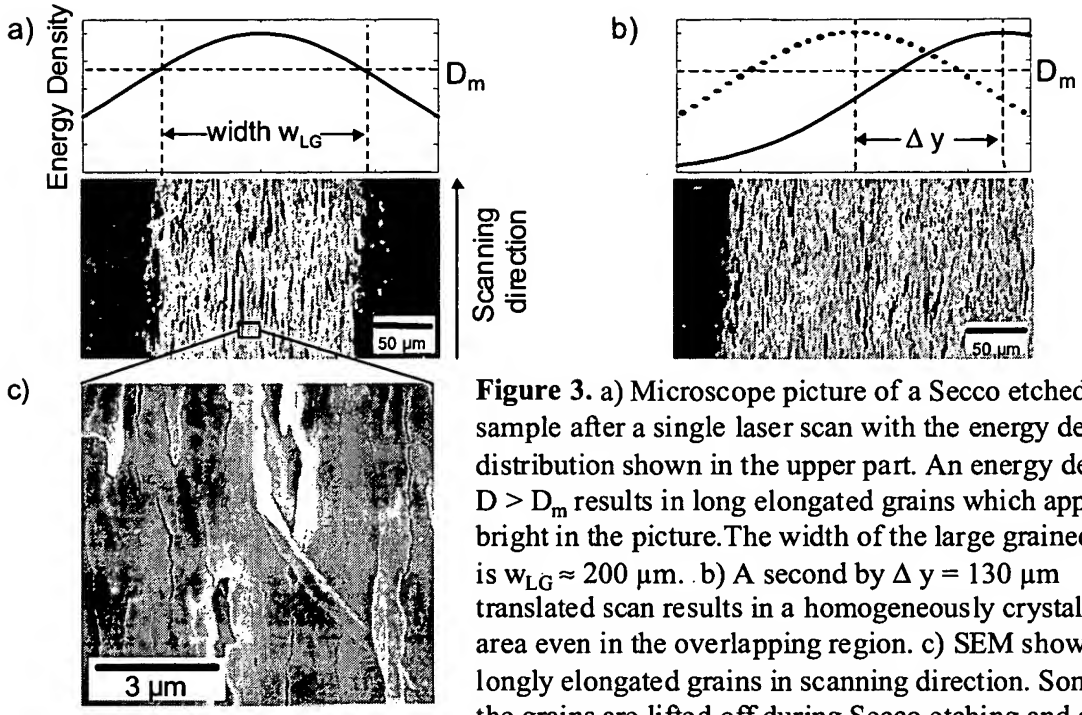

Figure 3. a) Microscope picture of a Secco etched sample after a single laser scan with the energy density distribution shown in the upper part. An energy density $D > D_m$ results in long elongated grains which appear bright in the picture.The width of the large grained area is $w_{LG} \approx 200$ µm. b) A second by $\Delta y = 130$ µm translated scan results in a homogeneously crystallized area even in the overlapping region. c) SEM shows longly elongated grains in scanning direction. Some of the grains are lifted off during Secco etching and appear dark in the microscope pictures a) and b)

3a. Figure 3b shows the energy density distribution of two subsequent scans with the translation $\Delta y = 130$ µm between them and the resulting microscope picture after Secco etching. The crystalline structure is the same throughout the whole crystallized area, even in the overlap region. The homogeneity in this region a result of two different crystalline growth mechanisms: i) In the region with $D > D_m$, the laser pulse completely remelts the large grained silicon produced by the previous laser scan. During the cooling, lateral growth again results in long grained material. ii) In the outer part of the beam the energy density $D < D_m$ is not high enough to completely melt the large grained silicon produced by the previous scan. The result is a liquid film on top of the remaining crystallites. Now these crystallites act as seed for columnar growth of the grains which rebuilds the previous grain structure.

Scanning electron microscopy validates that the bright areas of Figs. 3a, 3b correspond to the laterally elongated grains. The picture height is equal to the channel length $l_{CH} = 15$ µm of the TFTs we produce from the laser crystallized silicon. The grain length exceeds the channel length of the devices.

TFT Results

We fabricate TFTs with a channel length $w_{CH} = 15$ µm parallel to the scanning direction and a width $w_{CH} = 30$µm (for details see Ref. [7]). Figure 4 shows typical drain current (I_D) versus gate voltage (U_G) characteristics of p- and n-channel TFTs. The average electron and hole field effect mobilities of the n-channel and p-channel devices are $\mu_n = 467$ cm^2/Vs and $\mu_p = 217$ cm^2/Vs respectively. A comparison of these results with transistors produced by the same TFT process but with silicon from conventional excimer laser crystallization [7] shows the distinct

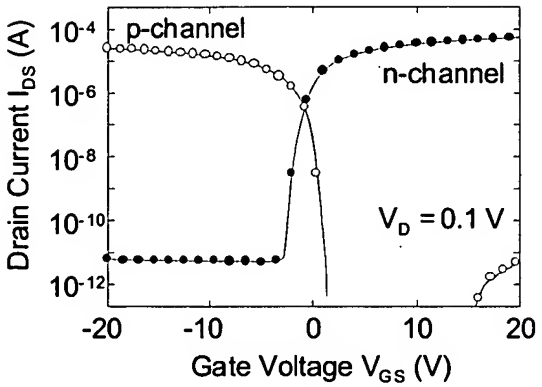

Figure 4. Transfer characteristics of n- and p-channel TFTs. The average mobilities are μ_n = 467 cm²/Vs and μ_p = 217 cm²/Vs respectively. The corresponding threshold voltages are V_t = 0 V ± 0.5 V and V_t = -1.8 V ± 0.5 V.

influence of the improved film quality: Applying the SLS process increases the grain length from approximately 1 μm to more than the channel length and enhances the electron mobility from $\mu_n \approx 150$ cm²/Vs to $\mu_n \approx 467$ cm²/Vs. Apart from a high mobility the *scatter* in the electrical properties is important for applications. Due to the homogeneity of the laser crystallized films we are able to produce devices with a standard deviation of the field effect mobility of only 5%.

CONCLUSIONS

We have developed a laser crystallization process based on sequential lateral solidification of amorphous silicon utilizing a solid state Nd:YVO_4 laser system. This process yields large-grained polycrystalline silicon with excellent electronic properties. We produced TFTs from crystallized samples with a silicon thickness d = 150 nm. These devices demonstrate high field effect mobilities of μ_n = 467 cm²/Vs and μ_p = 217 cm²/Vs for n- and p-channel devices respectively. The small standard deviation of the field effect mobility of only 5% is remarkable and a consequence of the high homogeneity and reproducibility of our laser crystallization process. An increasing repetition rate, going hand-in-hand with an increasing scanning speed, not only yields a higher throughput but also results in larger grains. Increasing the repetition rate should therefore further improve the electronic properties of the devices produced from crystallized films.

REFERENCES

1 M. Stehle, J. Non-Cryst. Solids **218,** 218 (1997).
2 A. T. Voutsas, A. M. Marmorstein, and R. Solanki, J. Electrochem. Soc. **146,** 3500 (1999).
3 A. Kohno, T. Sameshima, N. Sano, M. Sekiya, and M. Hara, IEEE Trans. Electron. Devices **42,** 251 (1995).
4 J. Levinson, F. R. Sheperd, P. J. Scanlon, W. D. Westwood, G. Este, and M. Ryder, J. Appl. Phys. **53,** 1193 (1982).
5 G. K. Giust, and T. W. Sigmon, Appl. Phys. Lett. **70,** 767 (1997).
6 R. S. Sposili, and J. S. Im, Appl. Phys. Lett. **69,** 2864 (1996).
7 Y. Helen, K. Mourgues, F. Raoult, T. Mohammed-Brahim, O. Bonnaud, R. Rogel, S. Prochasson, P. Boher, and D. Zahorski, Thin Solid Films **337,** 133 (1999).
8 R. Dassow, J. R. Köhler, M. Grauvogl, R. B. Bergmann, and J. H. Werner, Solid State Phenom. **67-68,** 193 (1999).
9 unpublished.
10 J. S. Im, and H. J. Kim, Appl. Phys. Lett. **63,** 1969 (1993).